Photocorrosion of n-GaAs and Passivation by Na_2S: A Comparison of the (100), (110), and (111)B Faces

E. A. Miller and G. L. Richmond

Department of Chemistry and Materials Science Institute, University of Oregon, Eugene, Oregon 97403

The Journal of Physical Chemistry B®

Reprinted from
Volume 101, Number 14, Pages 2669–2677

Photocorrosion of n-GaAs and Passivation by Na_2S: A Comparison of the (100), (110), and (111)B Faces

E. A. Miller and G. L. Richmond*

Department of Chemistry and Materials Science Institute, University of Oregon, Eugene, Oregon 97403

Received: September 18, 1996; In Final Form: January 7, 1997[⊗]

Photocorrosion of n-GaAs and passivation by Na_2S have been studied in a working photoelectrochemical cell as a function of crystal face orientation. Time-resolved photoluminescence studies of the (100), (110), and (111)B faces of n-GaAs show that Na_2S provides a similar degree of corrosion protection to the (100) and (110) faces, although the corrosion-induced surface states eventually formed at each interface are separated in energy by ~300 meV. Unlike (100) and (110), the (111)B surface is not passivated by Na_2S. The high density of intrinsic surface states at the (111)B n-GaAs surface, and the lack of removal of these states by Na_2S, pins the Fermi level and prevents trap saturation. X-ray photoelectron spectroscopic studies of the three surfaces before and after Na_2S treatment show a significant degree of arsenic sulfide bonding on (100) and (110). The (111)B face shows very little As−S bonding, indicating that formation of interfacial sulfides plays an important role in the reduction of interfacial traps and passivation of the photocorrosion reaction.

Introduction

GaAs has held great interest for use in semiconductor/liquid junction photoelectrochemical solar cell applications due to its high absorption near a maximum in the solar energy spectrum. The development of such devices has been hampered, however, by photocorrosion of the semiconductor photoelectrode. A large body of work has accumulated that addresses the problems of photocell stability and efficiency, not only in an effort to find a stable combination of semiconductor and electrolyte but also to understand the basic chemical processes occurring at the interface.[1,2] In the case of photocorrosion of n-GaAs, it is thought that holes driven to the interface oxidize surface bonds, causing an increase in the minority carrier surface recombination velocity (SRV) and ultimately a decrease in device lifetime and efficiency. Passivation of surface trap formation has been demonstrated by a variety of methods. Sandroff and co-workers[3] first observed the passivating effect of aqueous Na_2S on surface recombination centers of n-GaAs in air. Unfortunately, the passivation of surface traps on n-GaAs by Na_2S is not permanent and eventually gives way to corrosion.[4] Nevertheless, the n-GaAs/Na_2S system is among the most promising due to the passivation of surface recombination centers by the electrolyte itself, with no need for additional surface treatment.

In the search for an efficient semiconductor/liquid (SC/L) junction photoelectrochemical cell (PEC), various combinations of materials have been studied and treatments attempted for passivation of GaAs as well as other semiconductors. For example, studies have been performed on the effects of various inorganic sulfides on the SRV of GaAs,[5] the effects of other chalcogenides on GaAs surfaces,[6,7] the effects of metal ion adsorption on GaAs surface recombination,[8] and the effects of electrolyte composition on GaAs surface recombination[9] as well as similar studies on CdSe systems[10] and InP systems.[11] In the work presented here the focus is on comparison of photocorrosion, photowashing, and passivation of three different low-index crystal faces of GaAs. Correlations are made between the different chemical processes that occur at the different faces and the effectiveness of surface passivation.

Our approach to studying these systems has been to use several methods of measurement, both in-situ and ex-situ. The in-situ measurements, time-resolved photoluminescence spectroscopy (TRPL), and photocurrent (PC) spectroscopy allow dynamic effects in the working cell to be measured. Time-resolved photoluminescence (PL) decays measured at a variety of potentials from accumulation to depletion provide qualitative trends which reflect the degree of charge separation, band bending, and trap saturation. In addition, the decays can be used to determine whether chemical changes in the surface have any effect on carrier dynamics. PL decays measured at the flat-band potential can be fitted to obtain the SRV.[12,13] Because surface recombination is the most significant problem associated with development of photoelectrochemical solar cells, and because the SRV is a direct quantitative measurement of surface recombination, this quantity is of central importance in characterizing a given interface. In addition to the PL decays, the voltage dependence of the PL and PC is also measured as a function of sample exposure to laser irradiation. Changes in these quantities reflect changes in surface properties resulting from such processes as photocorrosion and photowashing. Studies of these surfaces ex-situ have been conducted with X-ray photoelectron spectroscopy (XPS) and TRPL measurements. XPS allows the determination of chemical products whereas TRPL assists in understanding the effect of surface chemical composition on carrier dynamics. Core level photoelectron peak energies are sensitive to the local bonding environment and can be used to differentiate between surface oxides, sulfides, or other surface substituents,[14] making XPS an ideal complement to the in-situ studies.

Photocorrosion has previously been observed in the n-GaAs/Na_2S system as an increase in the SRV and a decrease in PL.[4,9] It is thought that holes being driven to the surface oxidize the surface bonds, degrading and changing the surface, although it is unclear exactly what surface chemistry takes place and what surface products result. Upon photocorrosion, the primary observable effect is the introduction of additional surface states at a particular energy within the bandgap which increase the SRV at that energy.[4] Other observations of surface degradation include reduction in efficiency of oxidation of the redox couple (reduced photocurrent) and/or reduced absorption of incident light. The creation of additional minority carrier traps at the surface reduces the overall PL in the voltage region where those

[⊗] Abstract published in *Advance ACS Abstracts*, March 15, 1997.

S1089-5647(96)02852-0 CCC: $14.00

traps can be accessed and leads to an increased SRV in those regions.[4] The energy of the corrosion induced traps at the (100) n-GaAs/Na_2S interface is $E_c - 1$ V, where E_c is the energy of the conduction band edge. At voltages more positive of $E_c - 1$ V, the SRV is higher and the overall PL is lower than for an uncorroded sample. These corrosion induced states have previously been identified using capacitance techniques[15-17] and are fairly well characterized for the (100) surface. While a mechanism for the anodic dissolution of n-GaAs has been proposed,[18] the chemical mechanisms of photocorrosion and passivation are largely unknown.

The dependence of many material characteristics on the crystal face orientation is well-known. For example, surface electronic band structure,[19,20] surface reconstruction,[21] desorption kinetics,[22,23] and surface diffusion on metals[24,25] and semiconductors[26,27] have all been shown to be crystal face orientation dependent. There are also reactive differences found for different crystal face orientations, including catalysis, chemical etching rate,[28,29] photochemical unpinning rate,[30] and potential drop across an interface.[31] These studies suggest that it is not only the types of surface atoms that come in contact with solution which determine the interfacial chemistry but also the specific arrangement and electronic structure of these atoms. In this work, we have studied the photocorrosion of GaAs surfaces and passivation by Na_2S as a function of crystal orientation. The emphasis is on understanding how the specific interaction of S with surface Ga and As atoms affects photocorrosion and passivation. Our approach of studying the dynamic in-situ cell operation combined with ex-situ surface analytical techniques to determine interfacial products will help elucidate the forces that determine surface atomic interactions and should further the understanding of the passivation mechanisms.

Experimental Considerations

The Si-doped n-GaAs crystal wafers used in these studies were obtained from Crystal Specialties [(100) and (110)] and MCP Wafer Technology (111)B. The carrier concentrations were 6.2×10^{17} cm^{-3} for (100) and (110) and 2×10^{18} cm^{-3} for (111)B. The semiconductor electrode preparation was identical to that described in ref 13. Immediately prior to insertion into the electrochemical cell, each sample was etched (0.05% Br_2/MeOH followed by 1 M KOH, cycle repeated three times) to provide a clean, oxide-free surface. The sample was the working electrode in a standard three-electrode electrochemical cell, with a Pt wire counter electrode and a Ag/AgCl reference electrode. All potentials in this paper are referenced to Ag/AgCl unless otherwise noted.

The working electrode was illuminated at nearly normal incidence by the 532 nm frequency-doubled, pulse-compressed (~5 ps), focused output of a mode-locked Nd:YAG laser. The laser spot diameter at the electrode was ~150−200 μm. An acoustooptic modulator was used to reduce the laser repetition rate, and a half-wave plate/polarizer was used to adjust the power. To record photoluminescence decays, detection was done using the time-correlated single-photon-counting technique.[32] Luminescence was collected with *f*/2 optics and focused through a 610 nm long-pass filter into a monochromator set to transmit 855 nm. The monochromator output was detected by a microchannel plate photomultiplier tube, whose signal was then fed through a 1.8 GHz amplifier to a constant fraction discriminator. A time-to-amplitude converter (TAC) used the discriminator output as the start pulse, while a fast photodiode, which detects the laser pulse used to excite the sample, provided the stop pulse. The TAC output was recorded with a pulse height analysis program to give the luminescence decay. For clarity of presentation, the time axis on decay figures has been reversed.

Decay analysis is based on the equation

$$I(t)/I(0) = [(1/A)\exp(A^2T)\,\mathrm{erfc}(AT^{1/2}) - (1/S)\exp(S^2T)\,\mathrm{erfc}(ST^{1/2})][SA/(S-A)]\exp(-T) \quad (1)$$

where $I(t)$ is the PL intensity at time t, and A, T, and S are the reduced absorption coefficient ($\alpha(D\tau)^{1/2}$), reduced time (t/τ), and reduced SRV ($s(\tau/D)^{1/2}$), respectively. α is the absorption coefficient, τ is the bulk luminescence lifetime, s is the SRV, and D is the ambipolar diffusion coefficient.[12] As in our previous studies,[33] eq 1 has been modified to treat the surface recombination velocity (s) as a parameter that changes with time to reflect trap saturation and the resultant change in activation energy of trap occupation. The SRV, s, used in the above equation becomes

$$s(t) = s_0 \exp[-V((1 - \exp(-t/\tau_c))/k_bT_k)] \quad (2)$$

where s_0 is the initial surface recombination velocity, V is the trap barrier height at long times, τ_c is a time constant characterizing the evolution of the trap barrier height following laser pulse illumination, k_b is Boltzmann's constant, and T_k is the temperature. The value for α was calculated to be 78 421 cm^{-1} from measured values of the complex refractive index.[34] The van Roosbroeck−Shockley value of 6.4 ns was used for the bulk lifetime, τ.[35] The ambipolar diffusion coefficient was calculated, using literature values for the carrier mobilities, to be $D = 5.5$ cm^2/s, based on the doping density of the samples.[36] In performing the simulations, we chose the surface trapping velocity such that the early portion of the decay was reproduced, even without the inclusion of time-dependent trap barrier. In all cases, the early portion of the decay was found to be insensitive to the choice of the other parameters in eq 2, V and τ_c. The experimental decays were then simulated by adjusting V and τ_c. The cumulative uncertainty introduced by the many physical constants and variable parameters in the simulation preclude stating the precision of the measurements at better than a factor of ~2−3. The stated precision, therefore, reflects the sensitivity of the fit to only the SRV parameter, all other uncertainties held equal. This fitting procedure has previously been used to interpret our data taken at a range of photon fluxes and electrode biases, although it should be noted that the equations assume flat-band conditions.[13,33]

For the voltage-dependent photoluminescence scans, the PL intensity used was the valid conversion output (VCO) from the TAC, with a gate setting of 100 ns. The VCO was monitored as a function of time with a multichannel scaler as the electrode potential was scanned at a rate of 20 mV/s.

XPS data were obtained using a Kratos Analytical Axis HSI with a monochromatic Al anode X-ray source and hemispherical electrostatic electron energy analyzer. Samples were prepared by the aforementioned Br_2/MeOH/KOH etch procedure, followed by soaking in Na_2S for 12 h and a water rinse. An immediate transfer to XPS vacuum chamber was made with a total exposure time of the sample to ambient atmosphere of <30 s. The vacuum chamber was maintained at a pressure of ~2 $\times 10^{-9}$ Torr. Data collection times were on the order of 5 h.

Results and Discussion

A. In-Situ Studies. *I. (100) and (110) Faces.* As stated in the Introduction, it is known that photocorrosion at the (100) n-GaAs/Na_2S interface results in the formation of corrosion-

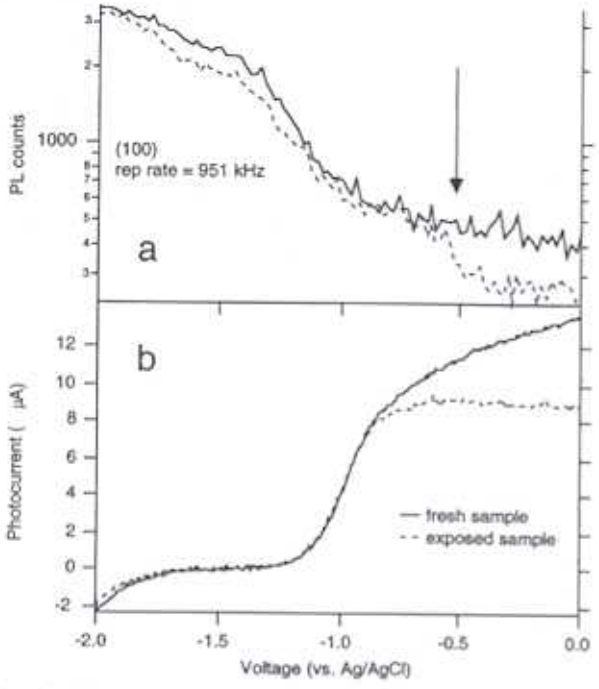

Figure 1. Photoluminescence and photocurrent as a function of applied voltage for (100) n-GaAs in 0.5 M Na_2S. Solid trace is response of freshly etched sample; dashed trace is after several voltage sweeps and laser exposure.

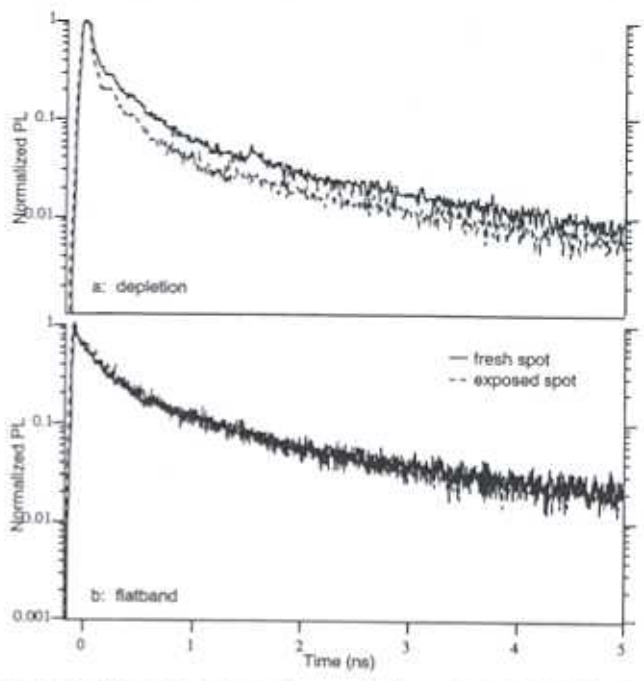

Figure 2. Photoluminescence decays of (100) n-GaAs in 0.5 M Na_2S. In (a) the electrode was held in depletion at $V = 0.0$ V; in (b) the electrode was held at flatband (−1.6 V). Solid traces are response of freshly etched electrode; dashed traces were obtained after corrosion of the sample.

induced minority trapping surface states as manifested in an observed increase in the SRV. The effects of photocorrosion are illustrated in Figure 1 where the photoluminescence and photocurrent data are plotted as a function of the applied voltage across the interface. Repeated cycling of the potential from $-2.0 \rightarrow 0.0 \rightarrow -2.0$ V was performed as the PL and PC were continually monitored. The laser repetition rate was 951 kHz, with a fluence of 8.0×10^{11} photons/(cm^2 pulse). The solid traces are the signal from a freshly prepared sample. The dashed traces are the signal from the same sample after extended exposure to high repetition rate laser radiation and continuous cycling of the potential. Initially, the sample behaves as would be expected, with the PL decreasing as the sample is biased into the depletion region and the PC increasing simultaneously. After extended exposure to the laser, photocorrosion causes a noticeable drop in the PL and PC signals which is consistently observed only at voltages positive of −0.5 V vs Ag/AgCl for the (100) surface. The PL and PC signal cathodic of this potential remain unchanged with laser exposure time and potential cycling. It was previously shown in this laboratory[4] that the corrosion which causes the decrease in PL in the depletion region is due to the creation of new surface states. Additionally, the studies showed that such corrosion occurs most readily under conditions where the intrinsic traps are saturated with minority carriers, i.e., high laser fluence and high excitation repetition rate. Such conditions resulted in the data shown in Figure 1. The additional traps reduce the degree of trap saturation by providing an additional nonradiative recombination pathway for the photoinduced carriers. Figure 1 shows that these new states are accessible only in a limited potential region, i.e., anodic of $E_c - 1$ V, providing an indication of their position within the bandgap.[4] The simultaneous drop in PC associated with corrosion indicates that these newly formed traps near $E_c - 1$ V are not charge-transfer traps but lead to nonradiative recombination.

PL decay measurements corroborate this interpretation. Figure 2a shows PL decays measured at the (100) n-GaAs/Na_2S interface with the electrode held at $V_{ap} = 0.0$ V, which is at a potential where the newly formed surface states can be accessed by carriers. The solid trace is from a freshly etched sample, and the dashed trace is from the same sample after corrosive laser exposure. The faster decay observed after the laser exposure shows that corrosion has created an additional nonradiative channel for carriers. PL decays were also measured before and after corrosion with the electrode held at V_{fb} ($V_{ap} = -1.6$ V vs Ag/AgCl) and are shown in Figure 2b. The fact that decays taken at flat band are identical before and after corrosion confirms that the corrosion-induced traps formed at this interface are only accessible when the Fermi level is at or below the energy of the traps.

Similar experiments have been performed on the (110) n-GaAs/NaS interface. Figure 3 shows the PL and PC as a function of voltage for a fresh sample (solid) and for a sample exposed to prolonged high repetition rate laser radiation (dashed). A dip in overall PL in the depletion region is observed, as on (100), indicating that extended laser exposure causes corrosion induced traps in a similar way as on (100). Although it is difficult to quantify the laser exposure necessary to see the effects of corrosion, it is consistently equal for the two interfaces. An important difference in the behavior of the two faces is the potential at which the dip occurs. The traps on (100) become accessible at an applied potential (V_{ap}) ≥ -0.5 V, or ~1 V below the conduction band edge. The onset of the PL drop on (110), however, is shifted anodic to that seen on (100), indicating that the corrosion-induced surface states formed on (110) are lower in the bandgap that those formed on (100) (Figure 4). The PC response from the (110) surface, which drops off at the same potential as did the PL signal, gives further indication that the nature of the corrosion states on (110) is similar to those on (100), although they are shifted lower in the bandgap. (It is possible that the apparent energy difference in the photocorrosion induced traps for the (100) and (110) faces is simply an artifact due to band movement/Fermi level pinning. Mott−Schottky analysis showed identical flat-band potentials and no band movement.)

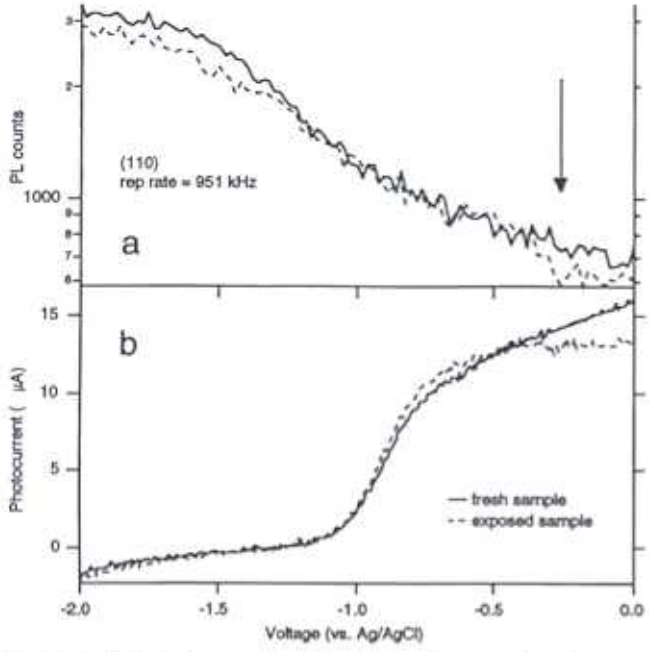

Figure 3. Photoluminescence and photocurrent as a function of applied voltage for (110) n-GaAs in 0.5 M Na_2S. Solid trace is response of freshly etched sample; dashed trace is after several voltage sweeps and laser exposure.

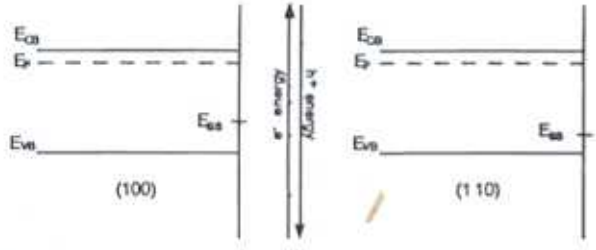

Figure 4. Diagram showing energies of corrosion-induced surface states for the (100)/Na_2S and (110)/Na_2S interfaces. Surface states induced on (110) are ~300 meV lower in the band gap than those formed on (100).

To further examine the nature of induced traps and to assess whether the drop in PL and PC with exposure is simply a result of formation of a polysulfide-type layer or other surface deformation that could conceivably lead to similar observations, the surfaces were examined under noncorrosive, nonsaturation conditions in which the laser repetition rate was reduced while the fluence remained unchanged (repetition rate = 238 kHz, fluence = 8.0×10^{11} photons/(cm^2 pulse)). For the remainder of this paper, "nonsaturation" laser exposure will refer to this fluence and repetition rate. For comparison, experiments were performed both on freshly etched samples and on samples that had been previously corroded with high repetition rate laser radiation. Figure 5 shows the voltage-dependent PL and PC data for a (100) surface.[4] The top set of scans (Figure 5a) is from a freshly etched sample; the bottom set (Figure 5b) is from a sample that had been previously corroded. As before, repeated cycling of the potential from $-2.0 \rightarrow 0.0 \rightarrow -2.0$ V was performed as the PL and PC were continually monitored. The solid traces are the initial scan in the experiment; the dashed traces are the last. The important feature in the data is that there is no drop in either PL or PC in the depletion region for the freshly etched sample under these low repetition rate conditions (Figure 5a). Furthermore, it is apparent that the corrosive exposure which preceded the bottom scans has not altered the way this sample behaves under nonsaturation conditions; i.e., both the PC and PL are identical to the fresh

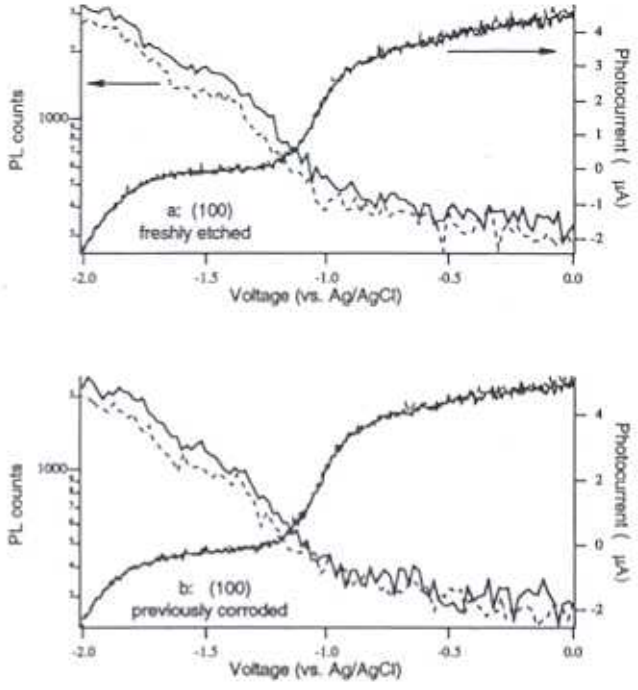

Figure 5. Photoluminescence and photocurrent as a function of applied voltage for (100) n-GaAs in 0.5 M Na_2S under low laser repetition rate (238 kHz) conditions. Solid trace is response of freshly etched sample; dashed trace is after several voltage sweeps and laser exposure. Top plot (a) is from a freshly etched sample; bottom plot (b) is from previously corroded sample.

sample. This indicates that high fluences are necessary not only to cause corrosion but also to access existing corrosion-induced traps. The results also suggest that trap formation is not accompanied by any physical deformation of the surface which would prevent absorption of the incident light.

The (110) surface exhibits very different behavior under low repetition rate, nonsaturation conditions. Voltage-dependent PL and PC data are shown in Figure 6 for a freshly etched sample and for a previously corroded sample. Figure 6a shows that both the PC and PL from a freshly etched (110) surface continually increase as laser exposure continues, eventually reaching a constant maximum. This behavior is in contrast to the stable behavior of (100) (Figure 5a) under the same conditions and is the reverse of what is seen during photocorrosion (Figure 3). An increase in PL with laser exposure has been attributed to the removal of surface states by photowashing.[37] We attribute the behavior observed for the (110) surface to a similar photowashing reaction.

To reiterate, all samples studied here have been chemically etched in an identical manner immediately prior to insertion into the electrochemical cell. Previous studies of GaAs have shown it to have an etch rate that is anisotropic with respect to crystal orientation.[28,29] Although the order of etch rate was found to be crystal face dependent, with an order of (110) > (111)B > (100) > (111)A, the result of such an etch is similar in terms of surface quality for all of the surfaces. Thus, we do not attribute any orientation-dependent experimental differences to etching differences. The data in Figures 5 and 6 show that under nonsaturation conditions (100) is relatively stable whereas (110) is prone to photowashing and suggest that it is the specific interaction of the different crystal faces with Na_2S which accounts for the different behavior. That is, while the different surfaces have been etched similarly and have oxide-free termination, the energetics of the bulk termination on (110) is such that interaction with Na_2S produces a high defect density. These defect states are removed by photowashing.

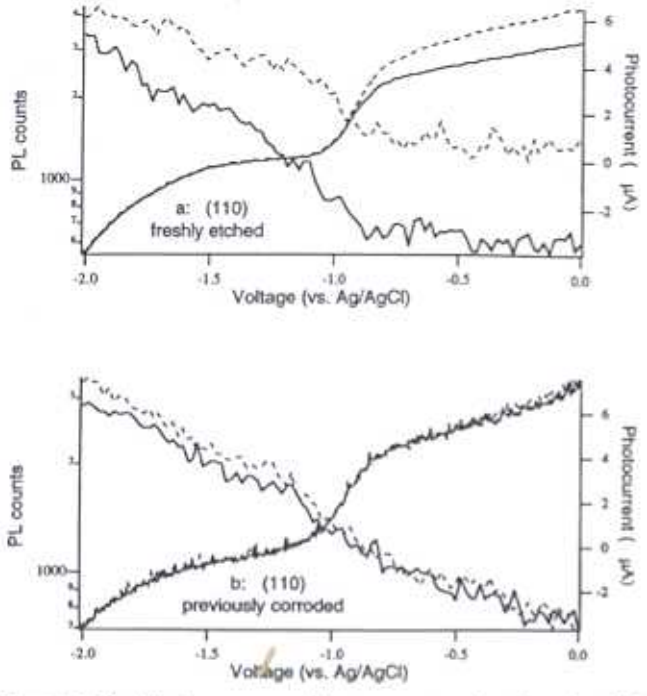

Figure 6. Photoluminescence and photocurrent as a function of applied voltage for (100) n-GaAs in 0.5 M Na_2S under low laser repetition rate (238 kHz) conditions. Solid trace is response of freshly etched sample; dashed trace is after several voltage sweeps and laser exposure. Top plot (a) is from a freshly etched sample; bottom plot (b) is from previously corroded sample.

The increases in PL and PC shown in Figure 6a for the (110) face eventually reach a maximum value and cease to increase further. If that surface is then exposed to corrosion-inducing illumination of high repetition rate laser light and then re-examined under nonsaturation conditions (Figure 6b), the result is a photocurrent that is the same as was seen from the photowashed sample before the corrosive exposure; i.e., the same high terminal PL and PC values are observed immediately with no increase or decrease with continued exposure. Also worth noting is that the corrosion-induced dip in PL and PC which is observed under high repetition rate exposure (Figure 3) is absent here under low repetition rate nonsaturation conditions (Figure 6b), as it was for (100) (Figure 5b), even though the sample has been corroded. Thus, whereas (100) and (110) are similar in their degree of susceptibility to corrosion at high laser fluences and in the nature of corrosion-induced states, there are important differences in the energy of the corrosion-induced states as well as in the behavior under nonsaturation conditions. These differences are the direct result of crystal face orientation.

Another useful parameter for characterizing the SC/L interface is the SRV measured at flatband potential (V_{fb}). Because there is no field present at the interface at V_{fb}, the SRV measured there reflects the "intrinsic" SRV, i.e., the ability of interfacial states to trap photogenerated carriers which have no driving force. (This is in contrast to the previously discussed corrosion-induced traps which are inaccessible unless the carriers have a driving force imparted by the applied voltage.) SRVs taken at V_{fb} have been measured from both (100) and (110) surfaces under all of the conditions previously employed in the PL and PC experiments to observe how these treatments affect the carrier trapping dynamics at the interface. Decays were measured from uncorroded surfaces under (1) high repetition rate (saturation) corrosive conditions, (2) low repetition rate (nonsaturation) before photowashing, and (3) low repetition rate (nonsaturation) after a photowashing treatment. (Here, a "photowashing treatment" is simply exposure to low repetition rate, nonsaturation irradiation while cycling the potential, similar to the conditions that led to the observations in Figure 6a.) The same experiments were then duplicated on samples that had been previously corroded. By fitting decays taken at V_{fb} to eq 1, we are able to obtain the SRV at V_{fb}. The results are summarized in the following tables. Table 1 shows the effects of corrosion, Table 2 shows the effects of photowashing on a freshly etched uncorroded sample, and Table 3 shows the effects of photowashing on a previously corroded sample.

TABLE 1: Effects of Photocorrosion on Freshly Etched Samples

	SRV ($\pm 0.05 \times 10^5$ cm/s)	
	(100)	(110)
before corrosion	1.13	1.41
after corrosion	1.12	1.34

TABLE 2: Effects of Photowashing on Freshly Etched Samples

	SRV ($\pm 0.05 \times 10^5$ cm/s)	
	(100)	(110)
before photowashing	1.13	1.41
after photowashing	1.12	1.12

TABLE 3: Effects of Photowashing on Previously Corroded Samples

	SRV ($\pm 0.05 \times 10^5$ cm/s)	
	(100)	(110)
before photowashing	1.12	1.34
after photowashing	1.12	1.34

There are several important features in the data which warrant discussion. The most prominent feature is that, for the (100) surface, neither the photocorrosion nor the photowashing pretreatments have had any effect on the SRV at V_{fb}. This is actually the expected result considering the PL and PC data already discussed. While photocorrosion does induce traps which are accessible in the depletion region (at $E_c - 1$ V), the fact that the PL dip in Figure 1 is well positive of V_{fb} would suggest that the corrosion-induced traps are not accessible at V_{fb}. Furthermore, because the photowashing treatment had no effect on the PL or PC for (100) at any potential, one would not expect to see any significant changes in the SRV at V_{fb} after photowashing.

Conversely, the (110) surface shows a complex response to the various pretreatments which is indicative of its more complex surface photochemistry. Considering first the experiments on uncorroded samples (Tables 1 and 2), several observations are noteworthy. First, the SRV from the as-etched (110) surface is significantly higher than that for (100), for both low and high repetition rate experiments. In general, a higher SRV under similar excitation conditions means a higher number of surface states or a higher trapping cross section. This indicates that the (110) surface has a higher density of intrinsic defects/trapping states than the (100) surface. Second, after a photowashing treatment, the (110) surface has the same SRV as a freshly etched (100) surface (Table 2). This is further evidence that, although both samples received an identical etch which results in an oxide free, well-terminated bulk, the (110)/Na_2S interface has a higher defect density and is thus more prone to photowashing. This photowashing reactivity apparently results in a surface comparable in quality to the as-etched (100) surface, as shown by its decreased SRV after the photowashing treatment. This result confirms the earlier result shown in Figures 5 and 6 for the voltage-dependent PL and PC experi-

ments where photowashing was seen on (110) but not (100). These results have implications on surface preparation methods. If one wishes to prepare a given interface to be in its lowest defect state, one must consider not only the types of materials that are to be in contact but also the crystal orientation of the materials.

The experiments on previously corroded samples are equally interesting (Table 3). The most striking feature of these data is that the SRVs from all previously corroded (110) surfaces are identical. Comparison of these results to those for samples that had not been previously corroded is very revealing. Because the dip in PL and PC which resulted from corrosion (Figure 3) is in the depletion region, one would not expect to see and change in SRV at V_{fb}. But, in fact, it has changed, from 1.41×10^5 to 1.34×10^5, indicating that the corrosion-inducing exposure may actually have slightly *improved* the surface as compared to the as-etched surface, but not to the same extent that photowashing improves the surface. Although corrosion is typically associated with surface degradation and an increased SRV, the resulting traps are not accessible at V_{fb}. Thus, the reduced SRV at V_{fb} is a result of some degree of photowashing which accompanies the corrosive high repetition rate exposure. This photowashing is not as complete as that induced by the low repetition rate photowashing, where the SRV was reduced from 1.41×10^5 to 1.12×10^5, indicating that the corrosion reaction interferes somewhat with the photowashing reaction.

An alternative interpretation of the photocurrent data in figure 6a is that the increasing photocurrent is due to photocorrosion, which is well-known to be a six-electron reaction.[38] The nature of the experiment, as well as the other evidence to the contrary, rules this interpretation out. The data in figure 6 were obtained over a period of ~10 min, with the potential being continually swept and laser exposure remaining constant. Only the first and last scans are shown. While a photocorrosion reaction does produce an instantaneous current 6 times that of a simple interfacial sulfide oxidation, the final result of photocorrosion is lower photocurrent due to the deterioration of the corroded interface.[4,9] Furthermore, while an instantaneous photocurrent jump accompanying photocorrosion is probable, to maintain that increase for the duration of the experiment would require consumption of a large amount of semiconductor material, a result which is not observed.

II. (111)B Face. The (111)B face of GaAs behaves very differently than the two faces already discussed. The differences are best understood in terms of saturation of intrinsic traps. For the (100) and (110) faces, corrosion is the result of saturation of intrinsic traps which causes the creation of corrosion-induced traps. Changes in decay rate as a function of excitation power have been previously shown for (100) to be a result of saturation of intrinsic traps[13] when the photon-induced charge injection is on the order of trap density. Here, PL decays were measured from the (111)B/Na_2S interface as a function of excitation power and are shown in Figure 7. Photon fluence ranged from 1.5×10^{11} to 1.5×10^{12} photons/(cm^2 pulse) at a repetition rate of 951 kHz. The data show identical decay rates over an order of magnitude of laser power, indicating that there is no change in the degree of trap saturation. This lack of trap saturation has been seen for unpassivated (100) samples examined in air, which are known to have a high density of surface traps. It can be concluded that Na_2S provides very little reduction or removal of interface traps from (111)B.

Experiments have also been performed that measure the potential dependence of PL decays from the (111)B/Na_2S interface. In the absence of Fermi level pinning, a change in interfacial potential results in a variation in PL decay rate as the depletion layer width is varied. At flat-band condition there is no field at the semiconductor surface, so photoinduced electron/hole pairs have no force separating them, and the result is slow decays. When the electrode is biased toward depletion, the field present at the surface separates electron/hole pairs, resulting in a faster decay rate. This effect has previously been demonstrated.[4] Shown in Figure 8 are potential-dependent PL decays for (111)B/Na_2S interface. Decays were measured at three potentials anodic of the flat-band potential. The lack of potential dependence of the PL decays is likely the result of Fermi level pinning, which results in the applied potential being dropped in the Helmholtz layer and surface states rather than in the space charge region. Because the applied potential would not be felt in the semiconductor, the depletion layer width would not change with applied potential, accounting for both the lack of power dependence and the lack of potential dependence of the PL decays.

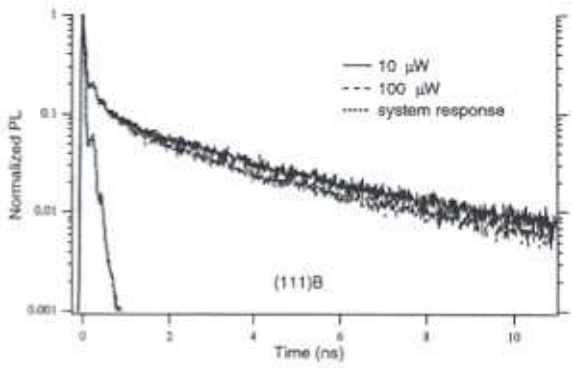

Figure 7. Laser power dependence of photoluminescence decays from the (111)B/Na_2S interface.

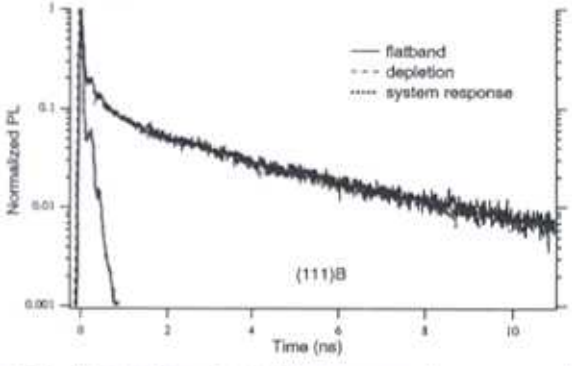

Figure 8. Dependence of photoluminescence decays on applied potential for the (111)B/Na_2S interface.

B. Ex-Situ Studies. The in-situ studies already discussed provide considerable information relating to how the cell behaves under operating conditions and how dynamic effects are manifested in changes in the PL, PC, and SRV. However, this information is somewhat incomplete in that it does not reveal much about the specific chemical interactions that result in the observed behavior. To obtain additional information about the chemical composition of the surface, we have performed X-ray photoelectron spectroscopy which is, by necessity, an ex-situ ultrahigh-vacuum technique. We have complemented these studies with ex-situ TRPL measurements which have been conducted in a similar manner to the in-situ TRPL previously discussed.

1. Ex-Situ TRPL. PL decays measured in air are very sensitive to the density of surface states; any change in this density resulting from chemical interactions will be evident. PL decays have been measured from untreated (native oxide

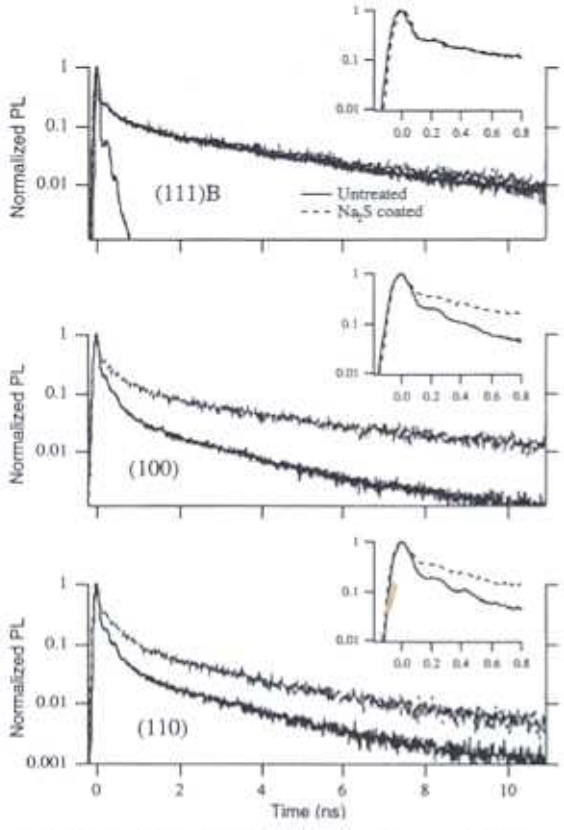

Figure 9. Ex-situ (air) photoluminescence decays. Solid traces are from untreated, unetched samples; dashed traces are from etched, Na_2S-coated surfaces. The system response is shown in the top plot.

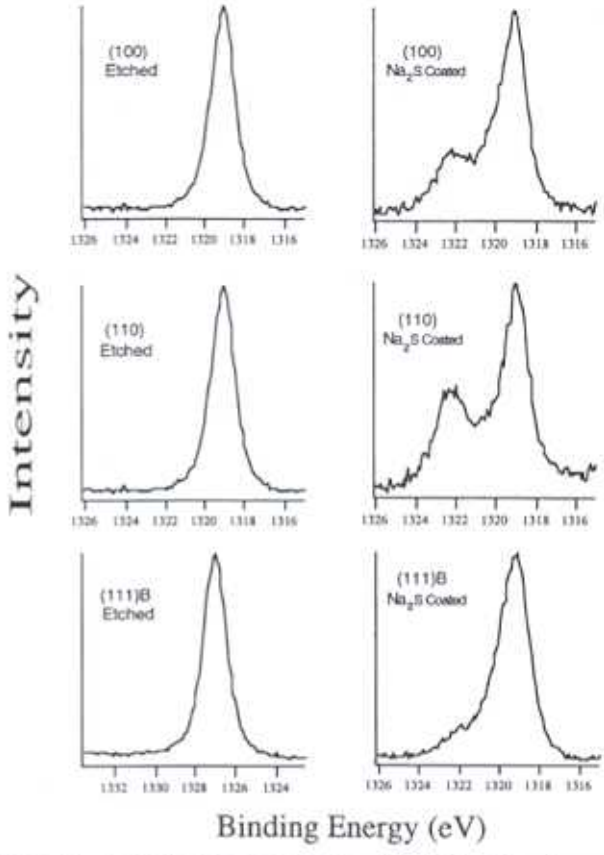

Figure 10. X-ray photoelectron spectra. Data in the left column are from etched samples; data in the right column are from Na_2S-coated samples.

covered) samples and from samples that had been chemically etched and soaked in 0.5 M Na_2S with the Na_2S allowed to dry onto the surface and are shown in Figure 9. All three untreated surfaces (solid lines) exhibit a very fast early decay component, with a long time component that asymptotically approaches an exponential decay. The early portion ($t < \sim 2$ ns) is sensitive primarily to changes in the SRV as found from performing data simulations using eqs 1 and 2, both in this study and in previous studies.[9,13] The latter portion of the decay ($t > \sim 4$ ns) is a far less sensitive indicator of changes in SRV and is sensitive primarily to variation of V and τ_c.

Upon coating the surfaces with Na_2S (dashed lines), the early portion of the decay is slowed considerably for the (100) and (110) surfaces, indicating that the Na_2S has removed surface states from these two surfaces, reducing the SRV. For the (111)B surface this effect is not observed, suggesting that Na_2S has no impact on the surface recombination velocity; i.e., Na_2S provides little, if any, removal of surface traps from the (111)B surface.

Alternatively, by comparing only the latter portions of the decays from the untreated surfaces, one might conclude that (111)B initially has a lower SRV which is subsequently not affected by the sulfide treatment. However, this explanation is inconsistent with the very fast decay observed for this surface in the first few nanoseconds, shown in the inset. It is also inconsistent with the fast SRV which was observed for this surface in solution, as discussed previously. Thus, we conclude that the intrinsic surface states on the (111)B surface are not removed by Na_2S, whereas they are removed for (100) and (110).

Yablonovitch and co-workers[5] have measured the effect of Na_2S on the density of recombination centers for the (100) n-GaAs surface using transient photoconductivity measurements and showed that the change in the decay was directly attributable to removal of surface states resulting in a reduction of the SRV by a factor of 25. We conclude from the data shown in Figure 9 that Na_2S interacts strongly with (100) and (110), significantly reducing their SRV, while it interacts very little with (111)B, leaving the intrinsic SRV unchanged. This conclusion is consistent with our in-situ experiments described earlier which showed that Na_2S does not provide the corrosion protection to (111)B that it provides to (100) and (110). (The fast early decay component present in the (111)B data is too fast to be modeled accurately using eqs 1 and 2. The upper limit of accuracy for the simulation is ~SRV < 350 000 cm/s. Thus, we put a lower limit on the SRV of the (111)B surface of 350 000 cm/s.)

II. X-ray Photoelectron Spectra. To further examine the nature of the differences in behavior exhibited by the different crystal faces, X-ray photoelectron spectroscopy was performed on the samples. The As 2p core levels were examined under several different sample preparation procedures to determine the extent of sulfide formation at the surface. The As 2p peak is known to be sensitive to the oxidation state and bonding environment of the surface As atoms.[14] Samples were prepared by first etching with Br_2/MeOH and KOH followed by immediate transfer to a Na_2S solution which was identical to the electrolyte used for the in-situ experiments previously discussed. After soaking the GaAs in the Na_2S solution for 12 h, the samples were subject to a running water rinse sufficient to eliminate any visible surface film, typically for about 5 s. Samples were then allowed to dry in a flowing N_2 atmosphere and subsequently transferred to the vacuum chamber. Samples rinsed for longer periods of time showed similar spectral features; those rinsed for shorter periods had a visible excess of Na_2S film which prevented the detection of the surface As XPS signal. For comparison, experiments were also performed on "clean" surfaces, those with no other surface substituents

other than the atoms that terminate the bulk. The clean surfaces were prepared by Ar^+ sputter etching in the XPS vacuum chamber. Data acquisition and sputtering were alternated until no further change was observed in the signal, indicating that any contaminants had been removed.

Spectra for (100), (110), and (111)B samples, both clean and Na_2S-treated, are shown in Figure 10. The most notable feature of the spectra is that the (100) and (110) samples show a prominent shoulder on the main As 2p peak after Na_2S treatment whereas this shoulder is absent for (111)B. It has been shown previously for the Na_2S-coated (100) surface of GaAs that this shoulder is due to the formation of arsenic sulfides.[14] Thus, it is clear from the data here that there is significant formation of arsenic sulfides on the (100) and (110) surfaces, while little or none are formed on the (111)B surface.

It was concluded from the optical experiments that Na_2S passivates the (100) and (110) surfaces from corrosion whereas (111)B is not passivated. The lack of passivation of (111)B was associated with a high SRV and surface trap density such that trap saturation by photoinduced charge carriers was not observed. The evidence from XPS is that As sulfides are formed on (100) and (110) but not on (111)B. We propose that the passivation mechanism involves the formation of sulfides at the interface and that this sulfide formation reduces the SRV.

Conclusions

The results presented here show that there are important differences in the photoelectrochemical behavior of the (100), (110), and (111)B faces of the n-GaAs/Na_2S PEC. Experiments that monitor PL and PC as a function of applied voltage show that Na_2S provides a similar degree of corrosion protection to both the (100) and (110) surfaces. However, the surface states eventually caused by corrosion are separated by several hundred millielectronvolts, those on (110) being closer to the valence band edge. These experiments, as well as time-resolved PL decays, also show that the etched (100) face is inert to any photowashing reactions in Na_2S, whereas (110), which has a higher initial SRV, is susceptible to photowashing in the cell, resulting in a reduction of surface states. The photowashing reaction reduces the SRV to a value identical to that for (100). The (111)B surface has a significantly higher SRV than either (100) or (110); passivation by Na_2S is not observed for the (111)B surface. XPS results show significant formation of arsenic sulfides on the (100) and (110) surfaces whereas (111)B showed little if any arsenic sulfide formation.

As mentioned in the Introduction, there are many examples of material properties and chemical reactions that are dependent on crystal face orientation, including catalysis, surface reconstructions, surface band structure, and molecular adsorption/desorption. Theoretical calculations predict that the position and density of surface states for Si, Ge, and GaAs will be orientation dependent,[20] a consequence of differences in rehybridization of surface orbitals, electronegativities of the atoms residing on the surface, and the resulting occupation of these surface orbitals. A common factor in all types of surface anisotropic processes is the energetics of the surface atoms with one another and the resulting interactions of these atoms with adsorbing and reactive species. In the analysis of the results presented here, it is instructive to examine the atomic arrangement of the three surfaces studied here (Figure 11). Only one type of atom is on the surface of (100) and (111)B, whereas both Ga and As atoms are on the surface of (110). Furthermore, the number of bonds each atom has with the bulk, and with other surface atoms, is different. A further consideration is the ionic or polar nature resulting from the III−V zinc-blende

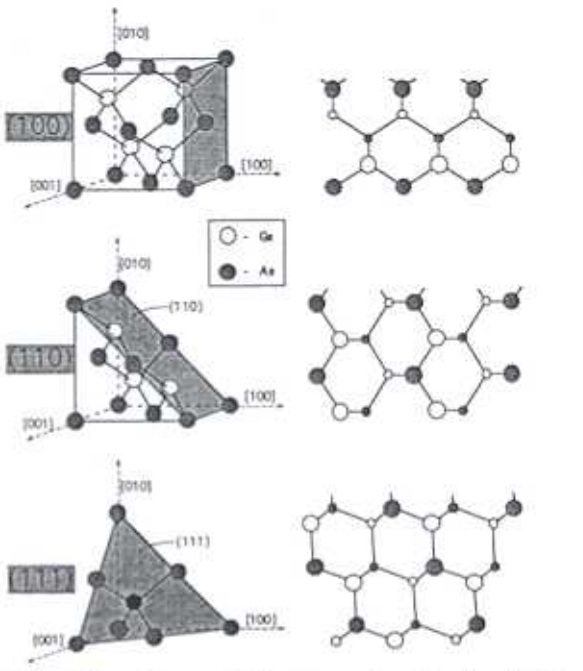

Figure 11. Ideal surfaces and 2-D cutaway view showing dangling bonds for the three low-index orientations studied.

structure of GaAs. These factors all contribute to very different energetics at these faces.

Based on the results shown in this work, specifically that (100) and (110) are passivated by Na_2S while (111)B is not and that arsenic sulfides form on (100) and (110) but not on (111)B, it is our conclusion that this arsenic sulfide formation is what provides the protection from photocorrosion. The passivation is accompanied by a removal of surface states. When bond formation occurs at a surface, the resulting energies of the new surface states will move away from midgap, toward the band edges, if the new bond is stronger then the one it replaces.[5,39] The (110)/Na_2S interface showed the largest degree of surface As−S formation as well as surface state formation at ~300 meV closer to the valence band edge than that of the (100)/Na_2S interface, which is consistent with our interpretation.

The likelihood of the reaction that produces the passivating arsenic sulfides is directly related to the atomic arrangement and resulting energetics of surface atoms. This can be made clear by examination of the (111)B/Na_2S interface. The ideal termination of the (111)B bulk results in a surface with a lone pair extending perpendicularly from the surface at every atom. While the termination of the etched surfaces is surely not ideal, the tendency of the surface toward this configuration will dominate the interfacial energetics. The species in solution that will participate in surface charge transfer are presumably the anionic NaS^- and S^{2-}. We suggest that it is the repulsive interaction between these species and the surface atoms which reduces the degree of As−S formation, as compared to (100) and (110), and thus prevents passivation of the (111)B surface. These results for (111)B are corroborated by a recent study done by Murphy et al.[40] Passivation of these surfaces is associated with removal of midgap surface states and unpinning of the Fermi level. From their synchrotron radiation photoelectron studies, in which they observed no movement of the Fermi level with sulfur adsorption in vacuum, Murphy et al. conclude that (111)B could not be passivated by sulfur. Further XPS analysis of Ga core levels as well as the lower binding energy levels of Ga and As, combined with similar studies of the (111)A surface, should provide further information regarding the role of bound sulfur in the passivation of n-GaAs.

Acknowledgment. The authors gratefully acknowledge the financial support of the Department of Energy, Basic Energy Sciences (DE-FG06-86ER45273). XPS instrumentation was obtained with a grant from the National Science Foundation (CHE-9512185).

References and Notes

(1) Heller, A. *Acc. Chem. Res.* **1981**, *14*, 154.
(2) Lewis, N. S. *Acc. Chem. Res.* **1990**, *23*, 176.
(3) Sandroff, C. J.; Nottenburg, R. N.; Bischoff, J. C.; Bhat, R. *Appl. Phys. Lett.* **1987**, *51*, 33.
(4) Balko, B. A.; Richmond, G. L. *J. Phys. Chem.* **1993**, *97*, 9002.
(5) Yablonovitch, E.; Sandroff, C. J.; Bhat, R.; Gmitter, T. *Appl. Phys. Lett.* **1987**, *51*, 439.
(6) Takatani, S.; Kikawa, T.; Nakazawa, M. *Phys. Rev. B* **1992**, *45*, 8498.
(7) Scimeca, T.; Watanabe, R.; Berrigan, R.; Oshima, M. *Phys. Rev. B* **1992**, *46*, 10201.
(8) Ryba, G. N.; Kenyon, C. N.; Lewis, N. S. *J. Phys. Chem.* **1993**, *97*, 13814.
(9) Balko, B. A.; Miller, E. A.; Richmond, G. L. *J. Phys. Chem.* **1995**, *99*, 4124.
(10) Benjamin, D.; Huppert, D. *J. Phys. Chem.* **1988**, *92*, 4676.
(11) Rosenwaks, Y.; Thacker, B. R.; Nozik, A. J.; Shapira, Y.; Huppert, D. *J. Phys. Chem.* **1993**, *97*, 10421.
(12) 't Hooft, G. W.; van Opdorp, C. *J. Appl. Phys.* **1986**, *60*, 1065.
(13) Kauffman, J. F.; Balko, B. A.; Richmond, G. L. *J. Phys. Chem.* **1992**, *96*, 6371.
(14) Lunt, S. R.; Ryba, G. N.; Santangelo, P. G.; Lewis, N. S. *J. Appl. Phys.* **1991**, *70*, 7449.
(15) Allongue, P.; Cachet, H. *Ber. Bunsen-Ges. Phys. Chem.* **1987**, *91*, 386.
(16) Allongue, P.; Cachet, H. *Ber. Bunsen-Ges. Phys. Chem.* **1988**, *92*, 566.
(17) Allongue, P. *Ber. Bunsen-Ges. Phys. Chem.* **1988**, *92*, 895.
(18) Schroder, K.; Memming, R. *Ber. Bunsen-Ges. Phys. Chem.* **1985**, *89*, 385.
(19) Ranke, W.; Jacobi, K. *Prog. Surf. Sci.* **1980**, *10*, 1.
(20) Ivanov, I.; Mazur, A.; Pollmann, J. *Surf. Sci.* **1980**, *92*, 365.
(21) D'Agostino, A. T.; Ross, P. N., Jr. *Surf. Sci.* **1987**, *185*, 88.
(22) Wise, M. L.; Koehler, B. G.; Gupta, P.; Coon, P. A.; George, S. M. *Surf. Sci.* **1991**, *258*, 166.
(23) Reider, G. A.; Hofer, U.; Heinz, T. F. *J. Chem. Phys.* **1991**, *94*, 4080.
(24) Xiao, X.-D.; Xie, Y.; Shen, Y. R. *Surf. Sci.* **1992**, *271*, 295.
(25) Zhu, X. D.; Rasing, T.; Shen, Y. R. *Phys. Rev. Lett.* **1988**, *61*, 2883.
(26) Vittadini, A.; Selloni, A.; Casarin, M. *Surf. Sci.* **1993**, *289*, L625.
(27) Reider, G. A.; Hofer, U.; Heinz, T. F. *Phys. Rev. Lett.* **1991**, *66*, 1994.
(28) Takebe, T.; Yamamoto, T.; Fujii, M.; Kobayashi, K. *J. Electrochem. Soc.* **1993**, *140*, 1169.
(29) Tarui, Y.; Komiya, Y.; Harada, Y. *J. Electrochem. Soc.* **1971**, *118*, 118.
(30) Ives, N. A.; Stupian, G. W.; Leung, M. S. *Appl. Phys. Lett.* **1990**, *56*, 1537.
(31) Rajeshwar, K.; Mraz, T. *J. Phys. Chem.* **1983**, *87*, 742.
(32) O'Connor, D. V.; Philips, D. *Time-correlated Single Photon Counting*; Academic Press: London, 1984.
(33) Kauffman, J. F.; Richmond, G. L. *J. Appl. Phys.* **1993**, *73*, 1912.
(34) Palik, E. D. *Handbook of Optical Constants of Solids*; Academic Press: Orlando, FL, 1985.
(35) Archer, M. D.; Bolton, J. R. *J. Phys. Chem.* **1990**, *94*, 8028.
(36) Orton, J. W.; Blood, P. *The Electrical Characterization of Semiconductors: Measurement of Minority Carrier Properties*; Academic Press: London, 1990.
(37) Kauffman, J. F.; Richmond, G. L. *Appl. Phys. Lett.* **1991**, *59*, 561.
(38) Gatos, H. C. *The Surface Chemistry of Metals and Semiconductors*; Wiley: New York, 1960.
(39) Bessler-Podorowski, P.; Huppert, D.; Rosenwaks, Y.; Shapira, Y. *J. Phys. Chem.* **1991**, *95*, 439.
(40) Murphy, B.; Moriarty, P.; Roberts, L.; Cafolla, T.; Hughes, G.; Koenders, L.; Bailey, P. *Surf. Sci.* **1994**, *317*, 73.
(41) Ohno, T. *Phys. Rev. B* **1991**, *44*, 6306.
(42) Moriarty, P.; Murphy, B.; Roberts, L.; Cafolla, A. A.; Hughes, G.; Koenders, L.; Bailey, P. *Phys. Rev. B* **1994**, *50*, 14237.
(43) Cierocki, K.; Troost, D.; Koenders, L.; Monch, W. *Surf. Sci.* **1992**, *264*, 23.
(44) Fan, J.-F.; Oigawa, H.; Nannichi, Y. *Jpn. J. Appl. Phys.* **1988**, *27*, L1331.